Research Square

Preprints are preliminary reports that have not undergone peer review.
They should not be considered conclusive, used to inform clinical practice,
or referenced by the media as validated information.

Flame retardant poly(ionic liquid) coating for polyethylene terephthalate fabrics: Improving anti-dripping performance with silica-containing flame retardant

Ailin Sun
Beijing Institute of Fashion Technology
Pengfei Qi
Beijing Institute of Fashion Technology
Wenqing Wang
20180021@bift.edu.cn

Beijing Institute of Fashion Technology
Yongmei Feng
Yantai University
Mengru Li
Beijing Institute of Fashion Technology
Menghan Guo
Beijing Institute of Fashion Technology
Yifan Yan
Beijing Institute of Fashion Technology
Zhiguo Zhu
Beijing Institute of Fashion Technology
Rui Wang
Beijing Institute of Fashion Technology

Research Article

Keywords: Flame retardant, UV irradiation grafting, Ionic liquid, Nano SiO_2, POSS

Posted Date: November 19th, 2026

DOI: https://doi.org/10.21203/rs.3.rs-11286132/v1

License: This work is licensed under a Creative Commons Attribution 4.0 International License.
Read Full License

Additional Declarations: No competing interests reported.

Flame retardant poly(ionic liquid) coating for polyethylene terephthalate fabrics: Improving anti-dripping performance with silica-containing flame retardant

Ailin Sun[a1], Pengfei Qi[a1], Wenqing Wang[a,b*], Yongmei Feng[c], Mengru Li[a], Menghan Guo[a], Yifan Yan[a], Zhiguo Zhu[a,b], Rui Wang[a,b]

[a]Materials Design & Engineering Department, Beijing Institute of Fashion Technology, Beijing 100029, China

[b]Beijing Key Laboratory of Clothing Materials R&D and Assessment, Beijing Engineering Research Center of Textile Nanofiber, Beijing Institute of Fashion Technology, Beijing 100029, China

[c]School of Chemistry & Chemical Engineering, Yantai University, Yantai 264003, China
*20180021@bift.edu.cn

Abstract: Poly(ionic liquid) (PIL)-based flame-retardant coatings were grafted onto polyethylene terephthalate (PET) fabrics by UV-initiated polymerization, using either physically dispersed nano-SiO_2 or copolymerizable polyhedral oligomeric silsesquioxane (POSS)as the silicon component. PET@PIL with a grafting add-on of 22.7 *wt*% lowered the peak heat-release rate (PHRR) by 25.5% and increased the cone-calorimeter residue by 126% relative to pristine PET, consistent with PIL-assisted dehydration and charring. Adding 25 *wt*% nano-SiO_2 to the combined PIL/silica solids reduced PHRR and total heat release (THR) by 38.7% and 12.7%, respectively, and eliminated melt dripping, yielding a UL-94 V-0 rating. At an IL/POSS molar ratio of 1:0.75, PHRR decreased by 32.8%, the limiting oxygen index reached 23%, and the fabric achieved V-0 without dripping. Char morphology and Raman results indicated that nano-SiO_2 reinforced an inorganic barrier, whereas covalently incorporated POSS promoted a more integrated silicon-containing network. TG-IR of the nano-SiO_2 system supported combined condensed- and gas-phase activity. These results clarify how silicon-source chemistry and bonding mode affect flame retardancy and anti-dripping behavior.

Key words: Flame retardant; UV irradiation grafting; Ionic liquid; Nano SiO_2; POSS

1. Introduction

Due to its good strength, high modulus, excellent elasticity, wear and impact resistance, polyethylene terephthalate (PET) has been widely used in many fields, including household products, automotive, packaging, electronics, health care, especially in the chemical fibers field, in which its market share is up to over 80%[1]. The melting point of PET fabric is about 260 ℃ with a limit oxygen index (LOI) of about 19%[2]. Severe melt droplets, accompanied by heavy smoke and toxic gas emissions, can occur during combustion, easily leading to large fire accidents and causing significant damage to personal and property safety[3]. Therefore, solving the inherent flammability of PET is of great significance for its safe and broad applications.

Up to now, many technologies have been applied to the fire resistance of PET, including copolymerization[4,5], blending[6], composite spinning[7], and surface modification strategies[8,9]. However, in blending methods, flame retardants (FRs) tend to clog the spinneret during spinning, while copolymerization involves complex synthesis processes and requires expensive equipment. Among the current flame retardant technologies, surface modification is a more feasible strategy with easy operation and high efficiency, and it offers advantages in fiber mechanical properties. To date, deposition, layer-by-layer self-assembly[10], spray[11], sol-gel and chemical grafting[12] have been applied, among which surface grafting has attracted much attention due to its good bonding between the functional layer and the substrate, improving the fastness and waterproofness of the flame retardant coating.

In recent years, photo-induced surface-initiated grafting polymerization has attracted much attention, in which light is employed as the main energy source and achieves chemical grafting of flame retardants onto the surface of the fabrics. It is expected to accomplish the design of a flame-retardant functional layer via effectively regulating the photo-initiated polymerization process with adjustable functional layer components, irradiation light intensity as well as time. UV irradiation polymerization is a common technology with easy operation and a high-energy donor to initiate the FRs polymerization, including phosphorus- and/or silicon-containing FRs, for example, diethyl (methacryloyloxymethyl) phosphonate(DEMMP)[13], oligomeric

silsesquioxane (POSS)[14], etc. Yang et al.[15] synthesized a novel UV-curable flame retardant monomer, EPPEM, containing phosphorus, nitrogen, and benzene rings, which formed a dense cross-linked network on the surface of PET blended fabrics to improve their flame retardancy and washing durability. The treated fabric showed an increased LOI value from 17.8% to 27.2% and maintained 26.6% after 25 laundering cycles. Wang et al.[16] synthesized a castor-oil-based bio-mercaptan (CO-SH) and an allyl-containing phosphorus FRs (DDP-AGE), which were combined with 2,4,6-trimethyl-2,4,6-trivinylcyclotrisilazane (TTC) through a thiolene click reaction to construct a UV-cured flame-retardant coating on wood. The coated wood achieved a UL-94 V-0 rating, an LOI of 27.52%, reduced heat and smoke release, and formed a compact char layer due to the synergistic flame-retardant effect of P, Si, and S.

For today, visible light-induced controlled polymerization is also proposed with lower energy consumption and better controllability. Hu et al.[17] prepared anti-UV and hydrophobic dual-functional coating fabrication for polyester (PET) fabrics based on surface-initiated photoinduced electron transfer reversible addition-fragmentation chain transfer polymerization (PET RAFT). The heat release of the fabric was effectively reduced, the UL-94 rating was V-0, and LOI was increased to 28%. Qi et al.[18] also used PET-RAFT technology for the controlled in-situ growth of a macromolecular flame retardant nano-coating for polylactic acid (PLA) fabrics through the copolymerization of diethyl(methacryloxy)methyl phosphonate (DEMMP) and 1-butyl-3-vinylimidazolium tetrafluoroborate ($VBImBF_4$) under yellow LED irradiation. Li et al.[19] grafted phosphorus-containing ionic liquids (ILs) onto PET fabrics via yellow LED-induced PET-RAFT polymerization, forming a 200-500 nm core-shell flame-retardant nanocoating. The modified fabrics showed excellent flame retardancy, smoke suppression, and anti-dripping behavior, with a 30.3% and 73.5% reduction in smoke release rate and total heat release, respectively, reaching UL-94 V-0 rating and an LOI of 28%.

Although much progress has been made in fire resistant finishing via photo-induced surface-initiated grafting polymerization, the properties of the FRs are the key component in the coating construction[18, 19]. Currently, a variety of FRs have been

reported, including halogens, phosphorus, nitrogen, boron, silicon, and multi-element systems [22]. Due to its eco-friendly and abundant molecular structures, phosphorus-based FRs are the most widely applied FRs type in fire protection PET synthesis, such as organic 3-hydroxyphenylphosphinyl-propanoic acid (CEPPA)[23, 24], [(6-oxido-6H-dibenz[c,e][1,2]oxaphosphorin-6-yl)methyl]butanedioic acid[25, 26] and 6H-dibenz (C,E) (1,2) oxaphosphorin-6-oxide (DOPO)[27, 28], inorganic ammonium polyphosphate (APP)[29], etc., playing efficient flame resistant roles in both gaseous and condensed states. Phosphorus-containing species that existed in the gaseous phase could capture H· radicals while the residual char was generated, promoting the formation of thermally stable carbon layers[30]. As reported, silicon-based FRs show good performance in smoke suppression and they also include organic, inorganic and organic-inorganic hybrid silicon-based FRs, such as SiO_2, cage octahedral oligosiloxanes, POSS, and so on[31,32]. For instance, zinc acetate and sodium silicate were used as two precursors in an aqueous ammonia solution to form ZnO@SiO_2 nanoparticles on PET fabrics at 90 °C. The SiO_2 carrier on the fabric's surface could effectively shorten the burning length of PET fabrics and improve the anti-melt-drop properties of PET fabrics during the burning process[33]. POSS is one kind of cage-like organic-inorganic hybrid silicone-based FR, which not only improved the flame retardancy and thermal stability of the material, but also effectively increased the mechanical and smoke suppression of the material[34]. Zhou et al.[35] reported a strategy for endowing PET fabrics with flame retardancy and smoke suppression properties through polyhedral oligomeric silsesquioxane (POSS)-functionalized polyglycidyl methacrylate (PGMA) coatings via initiators for continuous activator regeneration atom transfer radical polymerization (ICAR ATRP) technology.

Ionic liquid (IL) is well known as a “future solvent” and it has good chemical stability, non-flammability and environmental protection[36]. Owing to its structural designability, FR elements, such as phosphorus and boron, can be introduced into molecules to synthesize new flame-retardant materials with advantages of low mobility, high flame retardant element content and good compatibility with the matrix. At present, most of the existing flame-retardant ILs show good flame resistant behavior in various

substrates. Wang et al.[37] prepared a flame-retardant lignocellulosic composite by an IL activation-assisted hot pressing method. The IL-activated flame-retardant lignocellulose composite exhibited better flame retardancy and higher mechanical strength than pure lignocellulose. Wang et al.[38] prepared multifunctional cotton based on epichlorohydrin-modified aramid nanofibers (AEP), IL and $CuSO_4$ by using a simple layer dip coating method. Cot/AEP/IL/Cu showed lower flammability, and its maximum LOI increased from 18.5% to 28.5%, while PHRR decreased by 43.7% and THR decreased by 41.7%. Ou et al.[39] synthesized a novel phosphorus-containing IL (TPP-PF_6), which was used as a co-hardener of 4,4'-diaminodiphenylmethane (DDM) and a highly efficient FR of epoxy. It was found that TPP-PF_6 was beneficial in increasing char formation, thus inhibiting smoke release at high temperatures. Chen et al.[40] investigated the thermal degradation and flame retardancy of IL-modified graphene and hexaphenylcyclotriphosphonitrile in epoxy and found that a good dispersion of ILs in the matrix was observed, which promoted the char formation efficiency.

In this paper, commercial PET fabrics were selected as the matrix material. IL was employed as the main flame retardant, with silica-containing FRs (i.e., inorganic Nano SiO_2 and organic POSS), to fabricate multi-element flame-retardant coatings by UV-initiated free-radical grafting polymerization to improve the flame retardancy and melt-dripping of PET fabric. SEM-EDS, FTIR and TG characterized the morphology, structure, and thermal stability of the modified fabric. The flammability was investigated through LOI, UL-94 and CONE tests. The underlying flame retardant mechanism was studied through TG-FTIR and Raman tests.

2. Experimental

2.1 Materials

1-vinyl-3-butylimidazolium hexafluorophosphate ($C_9H_{15}F_6N_2P$, 99%) was purchased from Lanzhou Greenchem ILs (Lanzhou, China). Diphenyl(2,4,6-trimethylbenzoyl)phosphine oxide (TPO, 99%) and Dimethyl sulfoxide (DMSO, 99%) were both purchased form J&K Scientific Ltd. (Beijing, China). Nano silicon dioxide (Nano SiO_2, 99%) was purchased from Sigma-Aldrich (Shanghai, China).

Acrylolsobutyl Polyhedral Oligomeric Silsesquioxane (AB POSS, AR) was purchased from Hybrid (Shanghai, China).

2.2 Preparation of flame retardant PET fabric via UV-initiated grafting polymerization

2.2.1 Preparation of PET@PIL

In this paper, commercial pure PET was selected as the matrix material. Firstly, the PET fabric was pretreated. It was soaked in a 90 ℃ NaOH solution (concentration of 20.0 g/L) for 20 minutes, then washed once with detergent and ethanol, respectively, and finally washed with deionized water and dried at 100 ℃. Then, flame retardant finishing liquid with different concentrations of photo-initiator (TPO) and IL was prepared using DMSO as the solvent, and then the pretreated PET fabric was impregnated with the FR finishing liquid and rolled on a pad roller to get a certain liquid loading rate. Finally, the finishing solution was polymerized and grafted onto the fabric under a UV lamp at room temperature for 3 h. After the reaction, the fabric was washed with the reaction reagent twice, the solvent was volatilized in the fume hood, and then washed with deionized water three times. The fabric was dried in a vacuum at 80 ℃ and weighed. The grafting rate of polymer on the fabric surface is calculated by Eq. (1).

$$grafting\ rate\ (wt\%)=\frac{m_1-m_0}{m_0}\times 100\% \qquad \text{Eq. (1)}$$

where m_1 and m_0 are the quality of the modified and original fabrics, respectively.

The effect of initiator concentration, irradiation intensity, irradiation time, and irradiation distance was investigated. The FR finishing liquid was polymerized and grafted onto the fabric under UV irradiation, and the liquid carrying rate was 80%. The mass concentration of initiator TPO was set at 0.25 *wt*%, 0.5 *wt*%, 1 *wt*% and 2 *wt*%; irradiation intensity was adjusted to 0.15 mW/cm^2, 0.3 mW/cm^2, 0.45 mW/cm^2 and 0.6mW/cm^2, the reaction time was 1 h, 2 h, 3 h and 4 h, while the irradiation distance was 2 cm, 4 cm, 6 cm and 8 cm at room temperature. Based on the optimized conditions, PIL-finished PET fabrics were prepared and denoted as PET@PIL(*X*), where *X* was the grafting ratio of PIL.2.2.2 Preparation of PIL/Nano SiO_2 composite flame retardant coating

This method was the same as 2.2.1. Nano SiO_2 was incorporated into the flame-

retardant finishing solution at loadings of 15%, 20%, and 25% relative to the IL content using DMSO as solvent. The corresponding samples were denoted as PET@(PIL/Nano SiO_2(*X*)), where *X* was the weight ratio of Nano SiO_2 in the finishing solution.

2.2.3 Preparation of IL and POSS copolymerization flame retardate coating

This step was the same as 2.2.1, but it was slightly different in the preparation of the flame-retardant finishing liquid, which was to dissolve quantitative TPO, IL and POSS in DMSO. POSS was incorporated into the FR finishing solution at loadings of 25%, 50%, and 100% relative to the IL content. The corresponding samples were denoted as PET@(PIL-*co*-PPOSS(1:0.25)), PET@(PIL-*co*-PPOSS(1:0.5)), and PET@(PIL-*co*-PPOSS(1:0.75)), respectively. The synthesis schematic is shown in Fig. 1 and the detailed formulation is given in Table S1.

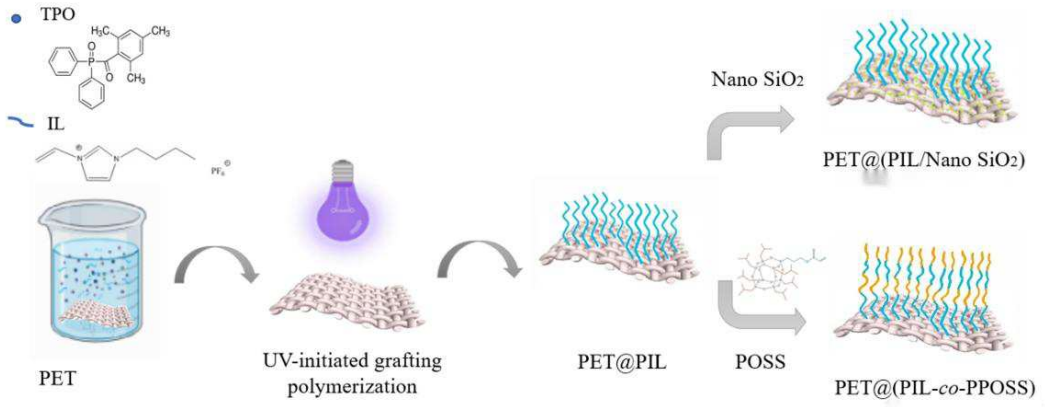


Fig. 1. Synthesis scheme of flame retardant PET fabric via photo-initiated grafting modification.

2.2.4 Characterizations

The morphology of the fabrics was observed using JEM2010 scanning electron microscopy (SEM) from Japan Electronics Co. Ltd. with an Oxford Instruments X-ray energy-dispersive spectrometer (EDS). Prior to each characterization, the samples were dried at 60 ℃ for 6 h in a vacuum, followed by conductive coating using a gold-palladium plasma spray for 20 s. Thermal stabilities were measured by a Netzsch TG 209 F1 thermogravimetric analyzer (TG/TGA) with a heating rate of 10 ℃ /min from 25 ℃ to 700 ℃ in an N_2 atmosphere. Chemical structure and characteristic functional groups of FRs were measured by Perseus TG 209 F1 in ATR mode; the spectrum

acquisition range was 4000-400 cm^{-1}, and the scanning frequency was 32 times. Element content was measured by an inductively coupled plasma spectrometer (ICP) from Agilent. Qualitative and quantitative element analysis was carried out by capturing the characteristic radiation emitted by the molecules of various elements to be measured in the excited state as they returned to the ground state, and the axial observation detection mode was selected. The combustion performance was tested in a British Fire Testing Technology Ltd Cone Calorimeter (CC). The samples were tailored into 100 mm × 100 mm and four layers were used at a thermal radiation power of 35 kW/m^2. The limiting oxygen index (LOI) values were tested using a Dynisco Oxygen Index Apparatus according to GB/T 5455-1997 and the specimens were cut into 150 mm × 58 mm; the Vertical Flame Test (VFT) was carried out using a GZF-3 Horizontal and Vertical Combustion Meter in reference to GB/T 5455-2014 and the samples were 300 mm × 89 mm. The degree of graphitization of carbon residue was measured by LabRAM HR Evolution (Raman) of HORIBA Jobin Yvon; the spectrum acquisition range was 3500-100 cm^{-1}, and the wavelength was 532 nm. The functional groups of the samples were analyzed using a Fourier transform infrared (FT-IR) spectrometer (Nexus 670, Nicolet) with a wavenumber between 500 and 4000 cm^{-1}.

3. Results and Discussion

3.1 UV irradiation polymerization of PIL onto PET fabric

The existence of initiators is a prerequisite for the realization of photo-initiated free radical polymerization[41]. The chain initiation stage of PIL can be expressed as follows: Firstly, the initiator was transferred from the ground state to the excited state under UV irradiation, generating TPO· free radicals, which reacted with the methylene that was bonded to the ester group of the PET main chain to generate C· free radicals. Subsequently, the PET macromolecular chain acted as the macroinitiator to trigger the IL monomer free radical, and then the PIL chain growth occurred and was grafted onto the PET chains. The effect of TPO concentration is shown in Fig. 2a and Table S2. The initiator series in Fig. 2a did not show a monotonic response: the grafting add-on increased from 3.84 wt% at 0.25 wt% TPO to 4.43 wt% at 0.50 wt%, decreased to 3.79 wt% at 1.00 wt%, and recovered to 4.17 wt% at 2.00 wt%. The small range and non-

monotonic behavior indicate competing effects of radical generation, solution-phase homopolymerization, and radical termination; therefore, these data do not justify a simple claim that more initiator always increases grafting. In this experiment, the optimal initiator concentration for PET fabric was determined to be 2 *wt*%.

UV light is the direct energy source for free radical generation and its intensity on IL polymerization grafting is shown in Fig. 2b. As seen from Fig. 2b, with the increase in irradiation intensity, the grafting rate of PIL gradually increased, reaching its highest within the experimental range (Table S3). Increasing nominal irradiance from 0.15 to 0.60 mW cm^{-2} increased the grafting add-on from 6.65 to 16.2 wt%. This was owing to the increased amount of excited-state TPO initiator at higher light irradiation energy, which stimulated the PET macromolecular chain to produce more active centers and promoted the free radical polymerization of the IL monomer.

The effect of irradiation time on IL polymerization grafting is shown in Fig. 2c. It can be seen from Fig. 2c that extending irradiation from 1 to 4 h increased the add-on from 4.83 to 8.96 wt%, as expected for continued radical polymerization. (Table S4). The irradiation time chosen was 3 h in this study. Similarly, the influence of irradiation distance on the preparation of the PIL-modified PET fabric is shown in Fig. 2d and Table S5. When the distance between the surface light source and the fabric was closer, the light intensity was correspondingly larger, which was conducive to an increase in the PIL grafting rate. But at the same time, high-intensity UV irradiation would also increase the degree of damage to fabric strength. In addition, from Table S5, it can be seen that the irradiation distance has little effect on the grafting rate of PIL on the fabric surface.

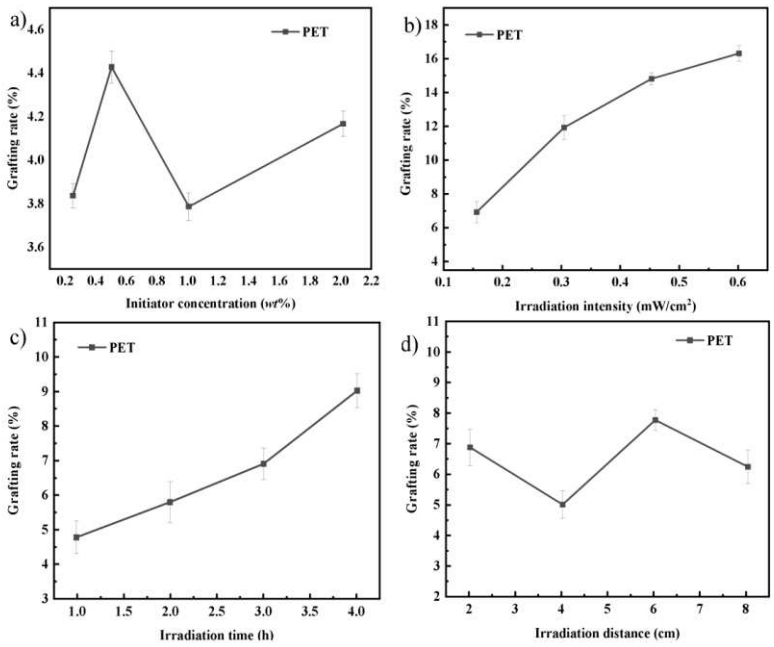


Fig. 2. Effect of different conditions on the grafting rate of PIL: (a) initiator concentration; (b) irradiation intensity; (c) irradiation time and (d) irradiation distance

3.2 Properties and characterization of UV irradiation polymerization grafted flame retardant PET fabrics

3.2.1 Surface morphology and elemental composition

The surface morphologies and elemental maps are shown in Fig. 3. Pristine PET retained a comparatively smooth fiber surface, whereas each modified fabric showed a continuous or particulate surface layer while preserving the woven architecture. P and F were detected on PET@PIL, consistent with deposition of the hexafluorophosphate-containing PIL. Si was detected on PET@(PIL/Nano SiO_2) and PET@(PIL-co-PPOSS), supporting the incorporation of the inorganic and organosilicon components, respectively. EDS is surface-sensitive and semi-quantitative; these elemental maps confirm the presence of the flame-retardant elements P and Si.

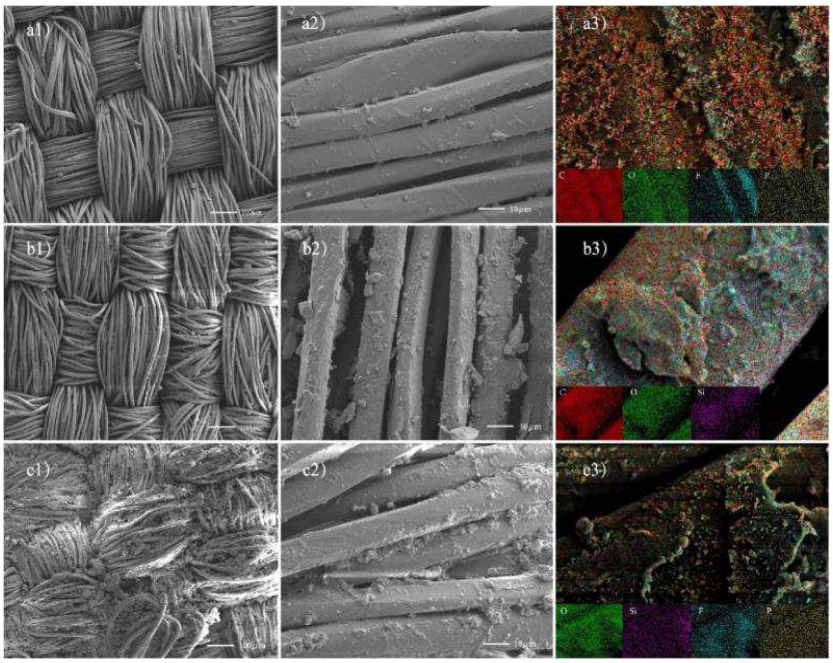


Fig. 3. SEM and SEM-EDS images at different magnifications: (a) PET@PIL; (b) PET@(PIL/Nano SiO_2); (c) PET@(PIL-*co*-PPOSS).

3.2.2 Structural and Constitutive Characterization

The FTIR spectra are shown in Fig. 4a. Pristine PET displayed the expected carbonyl, ester C-O-C, and aromatic C-H bands. After PIL treatment, changes near 1042 cm^{-1} were consistent with contributions from the grafted imidazolium-containing layer. The Nano SiO_2 and POSS-containing samples showed additional intensity in the 900-1100 cm^{-1} region, where Si-O-Si and Si- O- related modes overlap with polymer bands. The stretching vibration peak strength of the O-C=O bond at 2958 cm^{-1} increased significantly. The results showed that the content of ester groups in the sample increased, which was mainly due to the contribution of ester groups in the R side group of the POSS structure. In addition, the grafting of POSS reduced the peak intensity of the C-H bond and C=N double bond stretching vibration at 1711 cm^{-1}, further demonstrating that POSS was successfully grafted with PIL. Together with the EDS results, these spectral changes support coating formation and silicon incorporation.

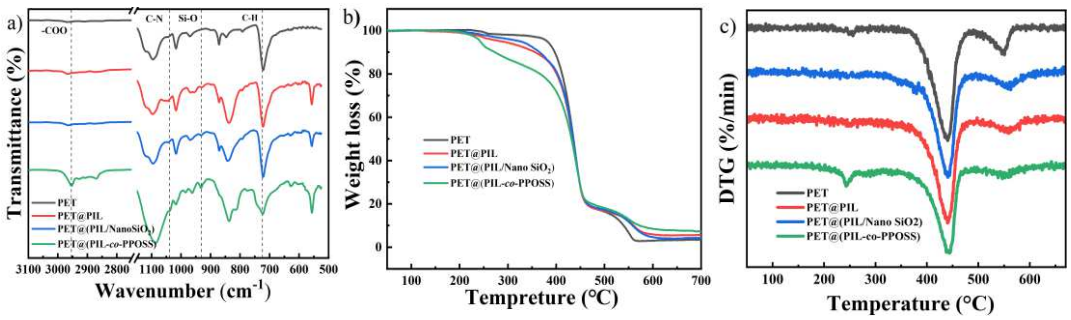


Fig. 4. (a) FTIR spectra of modified PET; (b)TG and (c) DTG curves of modified PET fabrics

3.2.3 Thermal stability

The TG and DTG curves of PET and its modified fabrics are shown in Fig. 4. As shown in Fig. 4b, compared with the original PET fabrics, the initial thermogravimetric temperature ($T_{5\%}$) of the modified fabric was lower, and its thermal stability decreased. This does not mean that the PET backbone underwent its principal decomposition at those temperatures. T_5% is defined for the total coated specimen; a small, less thermally stable coating fraction can therefore cause 5% mass loss before the main PET degradation step. To be specific, the initial decomposition temperature of PET@PIL ($T_{5\%}$=287 ℃) was about 95 ℃ earlier than that of PET, but the maximum thermogravimetric temperature (T_{max}) was essentially unchanged at about 440 ℃ compared with PET. The sample of PIL/Nano SiO_2 showed a similar trend compared to PET @ PIL with a slight increase in thermal stability. However, the $T_{5\%}$ value of PET@(PIL-*co*-PPOSS) decreased to 243 ℃, which was due to the low decomposition temperature of POSS in the copolymer. It was reported in the literature that the initial decomposition temperature of POSS was about 200 ℃, resulting in the advanced decomposition of modified PET. The maximum thermogravimetric peak shape of PET@(PIL-*co*-PPOSS) and the original PET fabrics basically remained the same (Fig. 4c), indicating that the IL/POSS copolymerization modified fabrics maintained the thermal stability of the matrix itself.

Table 1 shows the TG and DTG data of the PET fabric before and after modification. It can be seen from Table 1 that, compared with PET, the carbon residue rates of PET@PIL slightly increased, indicating that PIL had a certain charring property. After Nano SiO_2 introduction, the carbon residue ratio of PET@(PIL/Nano SiO_2) was

5.24 *wt*%, 2.19% higher than that of PET@PIL, which proved the effective contribution of the SiO_2 insulation layer. Similarly, the POSS and IL copolymerization FR system, i.e., PET@(PIL-*co*-PPOSS), also showed the char-promoting condensed phase effect of IL and POSS (residual char rate of 7.42 *wt*%). This is higher than the residual char rate of PET@(PIL/Nano SiO_2), indicating that the integrated copolymerization of organosilicon and IL has a greater catalytic carbonization advantage than simple mixing.

Table 1. TG data of PET and modified PET fabrics

Sample	Grafting rate (*wt*%)	$T_{5\%}$ (℃)	T_{max} (℃)	Residual char rate (*wt*%)
PET	-	382	440	3.07
PET@PIL	11.04	287	440	4.26
PET@(PIL/Nano SiO_2)	11.28	333	441	5.24
PET@(PIL-*co*-PPOSS)	14.07	243	443	7.42

3.2.4 Forced combustion

CC was used to compare ignition, heat release, smoke production, and post-combustion residue under an external heat flux of 35 kW m^{-2}. The heat-release rate (HRR), total heat release (THR), smoke-production rate (SPR), total smoke production (TSP), and final residue are summarized in Figs. 5 and 6 and Table 2. Increasing the PIL add-on altered both the magnitude and timing of heat release (Fig. 5a,b). At 22.7 wt% add-on, PHRR decreased from 613 to 456 kW m^{-2}, a reduction of 25.5% relative to PET. THR, however, remained close to that of PET (8.27 versus 8.11 MJ m^{-2}), and the time to ignition decreased from 80 to 21 s. The cone residue increased from 9.01 to 20.4 wt%, corresponding to a 126% relative increase. PIL therefore promoted condensed-phase residue and lowered PHRR, but it also caused earlier mass loss and did not substantially reduce the total heat released at the highest add-on.

In terms of smoke and gas release in the combustion process, it can be seen from the SPR curve in Fig. 5c that PIL reduced the smoke release rate in the PET combustion process. With an increase in grafting rate, the PSPR of PET@PIL showed a decreasing trend, but the TSP increased. The SPR value of PET reached the minimum value when the grafting rate of PIL was 22.73 *wt*%, and the pSPR decreased by about 22%.

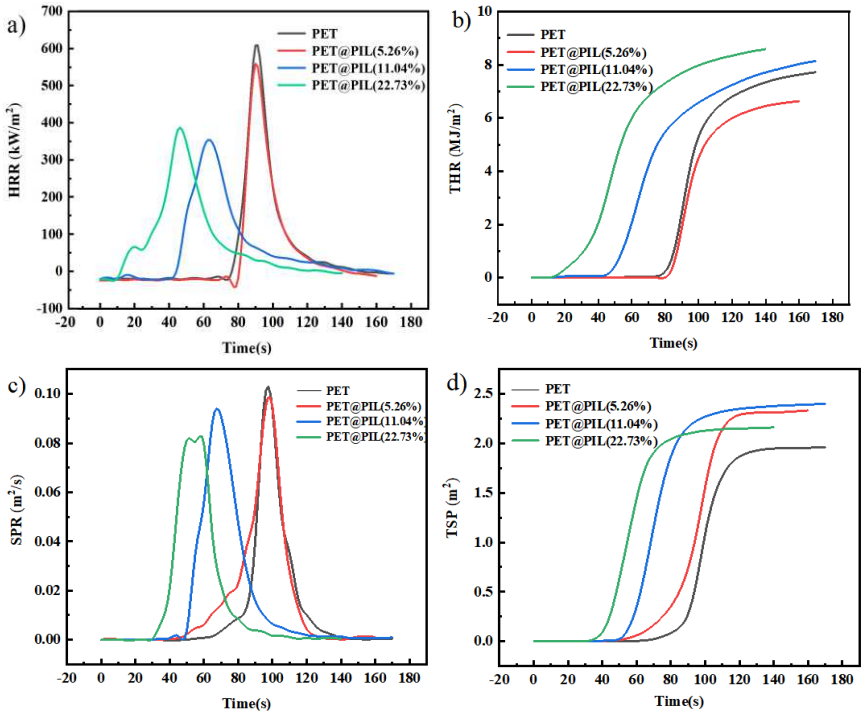


Fig. 5. CONE curves of PET and PET@PIL: (a) HRR; (b) THR; (c) SPR; and (d)TSP.

In order to further improve the flame retardant effect of IL-modified PET fabrics, the composite-modified PET samples with different concentrations of Nano SiO_2 and PIL were prepared. As seen in Fig.6, the combination of PIL and Nano SiO_2 decreased both the heat and smoke release of PET@PIL (Fig. 6a and 6b) and increased the amount of residual carbon (Table 2). The maximum THR and TSP of PET@(PIL/Nano SiO_2) decreased by 17.7% and 14.4%, respectively, compared with the pure 22.73 *wt*% PIL layer, exhibiting the physical barrier property of organic SiO_2. Although Nano SiO_2 could cooperate with PIL to provide superior heat suppression and smoke inhibition, the physically loaded Nano SiO_2 particles were prone to migration and poor washing fastness during UV-induced grafting and simultaneous nanoparticle deposition.

As shown in Fig. 6, the copolymerization of IL and POSS advanced the ignition time of PET fabrics, which may be attributed to the thermal decomposition of the organic groups in POSS. Compared with the PIL/Nano SiO_2 system, the PET@(PIL-*co*-PPOSS) coating showed a reduced reduction in heat release and smoke suppression due to the fact that POSS contained organic substituents and had a lower inorganic silicon content than Nano SiO_2. During combustion, these organic groups might generate additional volatile products, leading to an increase in THR compared with the

PIL-only coating. Nevertheless, the PHRR of PET@(PIL-*co*-PPOSS) was significantly reduced. At an IL/POSS molar ratio of 1:0.75, the PHRR decreased by 32.8% compared with that of pristine PET, suggesting that the integrated PIL-*co*-PPOSS coating could effectively delay and slow down the heat release process during combustion.

Although compared with inorganic Nano SiO_2, POSS showed certain disadvantages in heat release reduction and smoke suppression due to its organic structure and relatively weak inorganic barrier effect. However, its covalent incorporation into the PIL molecular chain enabled a more stable and integrated phosphorus–silicon-nitrogen synergistic flame-retardant network, which was beneficial for improving coating durability and reducing the fire risk of PET fabrics.

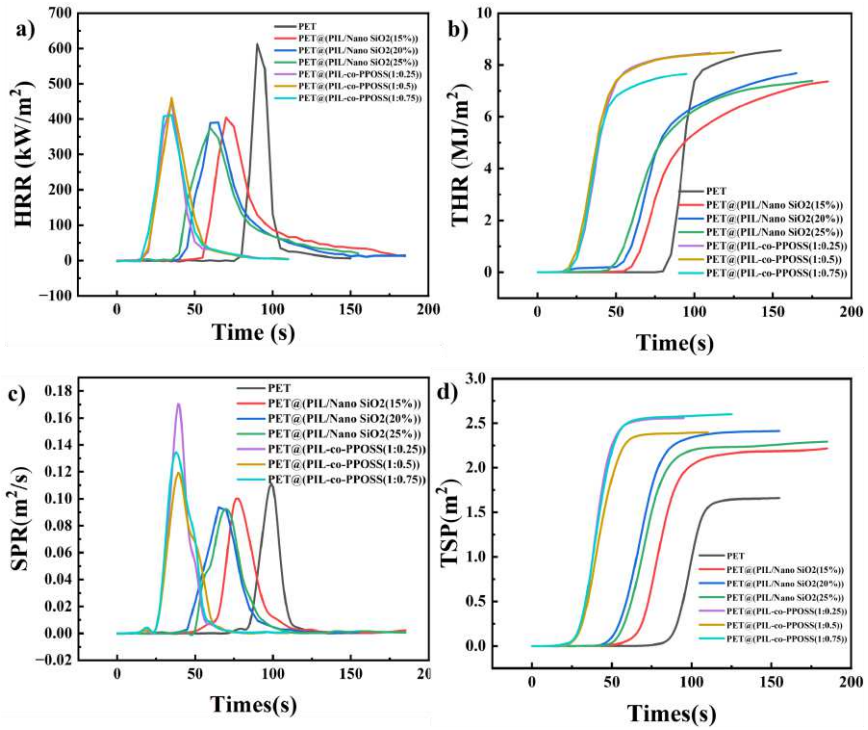


Fig. 6. CONE curves of PET, PET@(PIL/Nano SiO_2) with 15, 20, and 25 wt% Nano SiO_2, and PET@(PIL-co-PPOSS) at IL/POSS feed molar ratios of 1:0.25, 1:0.50, and 1:0.75: (a) HRR; (b) THR; (c) SPR; and (d) TSP.

Table 2. CC data for the pristine and modified FR fabrics

Sample	TTI(s)	PHRR (kW/m²)	THR (MJ/m²)	TSP (m²)	Residual char rate (*wt*%)
PET	80	613.08	8.11	1.80	9.01
PET@PIL(5.26%)	83	562.01	6.74	2.41	15.63

PET@PIL(11.04%)	50	417.67	7.90	2.45	16.86
PET@PIL(22.73%)	21	456.47	8.27	2.16	20.35
PET@(PIL/Nano SiO_2(15%))	59	404.90	7.80	2.15	19.26
PET@(PIL/Nano SiO_2(20%))	55	390.31	7.41	2.40	19.43
PET@(PIL/Nano SiO_2(25%))	48	375.58	7.08	2.27	20.60
PET@(PIL-*co*-PPOSS(1:0.2))	26	449.35	7.13	2.53	15.29
PET@(PIL-*co*-PPOSS(1:0.5))	25	461.14	7.93	2.37	15.13
PET@(PIL-*co*-PPOSS(1:0.75))	26	411.91	7.67	2.56	19.63

3.2.5 Flammability

The flame retardancy of the modified PET fabrics was evaluated by vertical burning (UL-94) and limiting oxygen index (LOI) tests, and the results are summarized in Table 3. With increasing PIL grafting ratio, the LOI value of PET@PIL slightly increased, and the damaged length after burning decreased, indicating that the PIL coating endowed PET fabrics with a certain degree of flame resistance. However, PET@PIL only achieved a V-2 rating in the UL-94 test due to the persistence of melt dripping. As shown in Table S6, the use of Nano SiO_2 or PPOSS alone also showed almost no flame-retardant effect, with a limiting oxygen index of only 20% and a UL-94 rating of only V-0.

After incorporating Nano SiO_2, the LOI value of PET@(PIL/Nano SiO_2) remained nearly unchanged, while the vertical burning behavior improved. When the Nano SiO_2 concentration reached 25 *wt*%, the melt droplets disappeared, and the fabric achieved a UL-94 V-0 rating. This improvement can be attributed to the formation of an inorganic Si-O-Si barrier layer, which enhanced the thermal shielding effect and partially suppressed melt dripping.

In contrast, for the PET@(PIL-*co*-PPOSS) system, POSS was covalently introduced into the PIL molecular chain to form an integrated P-Si flame-retardant network. Compared with the physically blended PIL/Nano SiO_2 system, the PIL-*co*-PPOSS coating exhibited a more effective synergistic flame-retardant effect because phosphorus and silicon were incorporated into the same macromolecular structure. When the feeding ratio of IL/POSS was 1:0.75, no melt dripping was also observed during combustion, and the modified PET fabric successfully achieved a UL-94 V-0

rating. Moreover, from the water-washing resistance test, it can be seen that PET@(PIL-co-PPOSS(1:0.75))-DIW still retains high flame retardancy (V-0), whereas the flame retardancy of PET@(PIL/Nano SiO_2(25%))-DIW decreases significantly (Table S6). This indicates that the formation of chemical crosslinking in the flame-retardant coating can improve the water-washing resistance of the coating.

Table 3. Results of LOI and UL-94 test for the pristine and PIL-functionalized PET fabric

Sample	Grafting rate (*wt*%)	LOI (%)	Melt droplet (12 s)	Cotton ignition	Damaged length （cm）	UL-94 Rating
PET	-	19	Yes	Yes	Burn through	N/A
PET@PIL(5.26%)	5.26	19	Yes	Yes	14.2	V-2
PET@PIL(11.04%)	11.04	20	Yes	Yes	13.2	V-2
PET@PIL(22.73%)	22.73	20	Yes	Yes	12.5	V-2
PET@(PIL/Nano SiO_2(15%))	12.28	20	Yes	Yes	13.0	V-2
PET@(PIL/Nano SiO_2(20%))	17.66	20	Yes	Yes	12.1	V-2
PET@(PIL/Nano SiO_2(25%))	16.15	20	No	No	10.1	V-0
PET@(PIL-*co*-PPOSS(1:0.25))	10.95	21	Yes	No	13.4	V-1
PET@(PIL-*co*-PPOSS(1:0.5))	16.29	22	Yes	No	12.8	V-1
PET@(PIL-*co*-PPOSS(1:0.75))	14.07	23	No	No	12.6	V-0

Note: For PET@(PIL/Nano SiO_2(25%), PIL:SiO_2=20:1(*wt:wt)*; For PET@(PIL-*co*-PPOSS(1:0.75), PIL:PPOSS=2.4:1(*wt:wt)*, which calculated from ICP test.

To further verify the hypothesis that silica-containing FRs could be effectively synergized with IL to get better anti-dripping performance and flame retardancy. Commercially available flame-retardant PET (FRPET) fabrics were introduced with higher copolymerized phosphorus content (6500 ppm). The LOI values for FRPER @(PIL/Nano SiO_2) and FRPER@(PIL-*co*-PPOSS) were 35% and 39%, respectively, and achieved a UL-94 V-0 rating (Table S7), demonstrating their superior vertical burning performance.

3.2.6 Char analysis

In general, the residual char layer played an important role as a protective barrier in flame-retardant systems, especially in condensed-phase flame-retardant mechanisms. As shown in Fig. 7, pristine PET exhibited a loose and discontinuous char residue with

large pores on the surface after combustion. These pores were mainly caused by the rapid decomposition of PET and the violent release of volatile pyrolysis products during burning. The escape of combustible gases and smoke destroyed the integrity of the char layer, resulting in a porous and fragile carbonaceous structure.

After PIL grafting, char layer formation was promoted, demonstrating the IL's catalytic carbonization ability. With the further introduction of Nano SiO_2, a denser char structure and improved char strength were obtained. However, relatively large pores could still be observed on the surface of PET@(PIL/Nano SiO_2). This may be attributed to the physical blending of Nano SiO_2 with the PIL coating, where interfacial incompatibility between the inorganic nanoparticles and the organic polymer layer limited the formation of a continuous and compact char network, which was speculated to be the SiO_2 that had not thermally decomposed. In addition, the rapid release of degradation gases from the PET substrate also contributed to pore formation in the residual char.

PET@(PIL-co-PPOSS) showed smaller and more uniformly distributed pores than PET@(PIL/Nano-SiO_2), consistent with more homogeneous distribution of the covalently incorporated POSS component. Its residue was still more porous than that of pristine PET at some magnifications, reflecting gas evolution from the organic substituents and the PET substrate. The images therefore support improved continuity relative to the physically blended coating, not a completely pore-free barrier.

Compared with Fig. 7d2 and Fig. 7a2, it can be seen that the pores of the char layer got larger after the *co*-polymerization of IL and POSS, which might be due to the flame retardancy role of POSS in the gas phase. Firstly, the Si element was oxidized to form the Si-O-Si structure, and during thermal decomposition, the Si-O bond was heated to form the Si-C bond, which could absorb a large amount of heat and become a protective coke layer. The Si-O bond was also confirmed from the infrared spectrum, with absorption peaks located at 950 cm^{-1} (Fig. S1). On the other hand, the N element in IL can be thermally decomposed into NH_3, N_2 and H_2O, non-flammable gases, which can effectively absorb heat and hinder the combustion reaction of the fabric. In summary, the POSS layer exerted a flame-retardant effect in both the condensed phase and the

gas phase, and had a protective effect on the underlying flame-retardant PET fabrics.

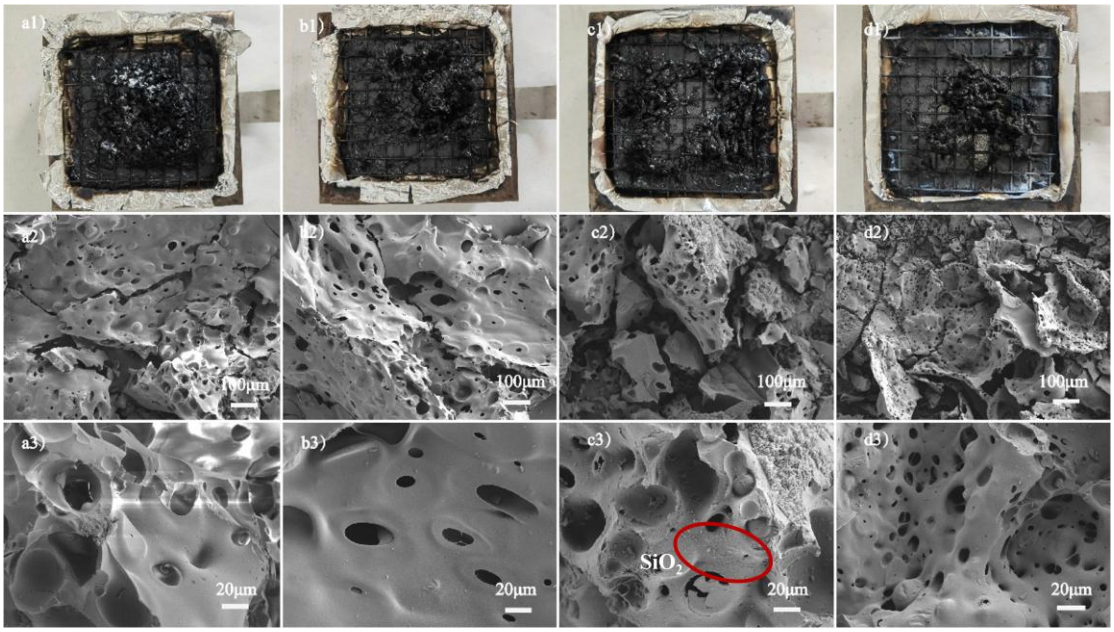


Fig. 7. Carbon residue of modified fabric and SEM images at different magnifications. (a)PET; (b) PET@PIL; (c) PET@(PIL/Nano SiO_2); (d) PET@(PIL-*co*-PPOSS)

To further study the degree of graphitization of carbon residue and the mechanism of the condensed phase of the modified sample, Raman test was performed on carbon residue, and the results are shown in Fig.8. The residual carbon of the samples showed two Raman characteristic peaks of C atomic crystals, representing the D band of amorphous carbon and the G band of graphitic carbon, respectively. The graphitization degree of the residual carbon is related to the quality of the protective carbon layer, which is usually described by the ratio of the combined intensity of the G and D bands (I_G/I_D). As seen in Fig.8, the I_G/I_D values of PET@(PIL/Nano SiO_2) and PET@(PIL-*co*-PPOSS) were 0.59 and 0.61, respectively, which were significantly higher than those of PET and PET@PIL (I_G/I_D=0.43 and 0.5, respectively), indicating that the degree of graphitization of fabric combustion residual carbon increased after polymerization grafting, and that both Nano SiO_2 and POSS made contributions in the improvement of char quality in the condensed phase, which was in agreement with the results of the aforementioned residual carbon analysis.

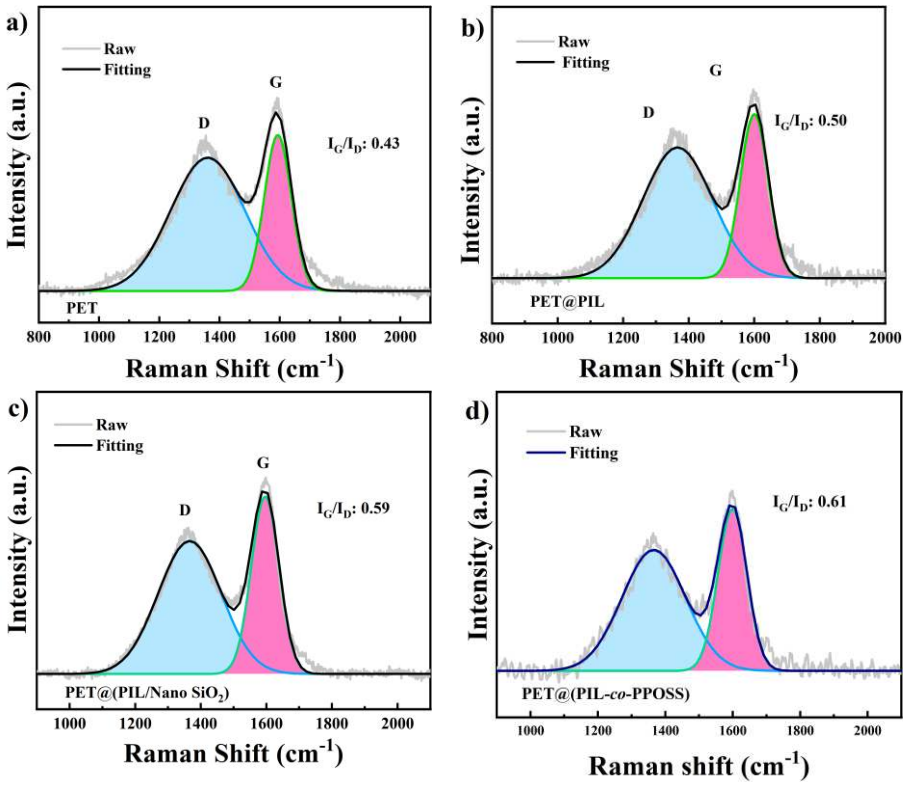


Fig. 8. Raman diagram of residual carbon (a) PET; (b) PET@PIL; (c) PET@(PIL/Nano SiO_2); (d) PET@(PIL-*co*-PPOSS)

3.2.7 Flame retardant mechanism analysis

To further elucidate the evolution of gaseous products during the thermal degradation of PET and its modified systems, TG-IR analysis was performed and the results are given in Fig.9. Two representative temperatures were selected to characterize the release behavior of volatile products. For the PET@(PIL/Nano SiO_2) sample, the strong absorption bands in the 1700-1800 cm^{-1} region were mainly assigned to carbonyl-containing compounds, such as esters, carboxylic acids, aldehydes, and ketones, indicating substantial cleavage of PET molecular chains and the release of oxygenated aromatic fragments. The absorption band near 1400 cm^{-1} was associated with carboxyl-related deformation vibration and partial alkyl bending vibration. In addition, the broad absorptions in the 1100–1250 cm^{-1} region were mainly attributed to the C-O-C vibrations of ester-derived pyrolysis products. The 943 cm^{-1} region of PO· was attributed to phosphorus-containing oxygenated fragments generated from PIL decomposition. After entering the gas phase, these phosphorus-containing active species could capture highly reactive H· and OH· radicals generated during combustion, thereby interrupting the flame chain reactions and suppressing flame propagation. The

absorptions in the low-wavenumber region of 700-900 cm^{-1} were assigned to the out-of-plane bending vibration of aromatic C-H, further confirming the continuous release of aromatic intermediates during the later stage of thermal degradation.

According to previous TG-IR studies on neat PET, the major volatile products of PET pyrolysis include carbon dioxide, acetaldehyde, vinyl benzoate, terephthalic acid, terephthalaldehyde, together with small amounts of benzoic acid and linear oligomers[42]. Moreover, the characteristic infrared bands of PET degradation products are mainly located at around 1730 cm^{-1} for carbonyl stretching, approximately 1250 cm^{-1} for ester C-O vibration, and in the 730 cm^{-1} region for aromatic substitution-related vibrations and aromatic C-H out-of-plane bending modes. The same study further showed that the non-volatile residue of PET gradually evolved into an aromatic-ring-rich structure during thermal degradation. These reported results are in good agreement with the absorption features observed for PET@(PIL/Nano SiO_2) in the regions of 1700-1800, 1100-1250, and 700-900 cm^{-1}, suggesting that the volatile products of the modified sample at high temperature still mainly originated from ester scission and oxygenated aromatic fragments derived from PET backbone decomposition.

Compared with neat PET, PET@(PIL/Nano SiO_2) exhibited broader and more intense absorptions in the 1100-1250 cm^{-1} region, indicating that the introduction of PIL altered the thermal degradation pathway of PET and promoted the evolution of phosphorus-containing oxygenated fragments in addition to the conventional ester-derived products. Nano-SiO_2 mainly remained in the condensed phase and acted as an inorganic barrier rather than directly contributing to gaseous products. Combined with the TG, cone calorimetry, and char residue analysis results, the increased char yield and the reduced THR and TSP of PET@(PIL/Nano SiO_2) demonstrated that the incorporation of PIL and Nano SiO_2 significantly enhanced the condensed-phase flame-retardant effect. It was found that PIL promoted dehydration, crosslinking, and carbonization during thermal decomposition, and may also release phosphorus-containing active fragments that contributed to flame inhibition. Meanwhile, Nano SiO_2 facilitated the formation of a more compact and thermally stable barrier layer, thereby

suppressing heat transfer and retarding the outward diffusion of combustible volatiles. Therefore, the improved flame retardancy of PET@(PIL/Nano SiO_2) can be mainly attributed to the synergistic effect of PIL-induced charring and SiO_2-enhanced barrier protection, which effectively reduced the release of combustible volatiles and reinforced the protective effect of the condensed-phase char layer.

The flame retardant mechanism of the modified PET fabric is primarily driven by the formation of a protective char layer that acts as a heat barrier, especially in a condensed-phase flame retardant strategy. The IL polymerization grafting promoted char generation, and the addition of silica-based FRs, Nano SiO_2 and POSS, in this study further strengthens and densifies the char layer. This char layer, along with an insulating silica coating, effectively interrupts heat transfer and smoke release, enhancing fire resistance. In the condensed phase, POSS and PIL formed Si-O-P bonds that absorb heat, while in the gas phase, the nitrogen in the IL releases non-flammable gases (NH_3, N_2, and H_2O) that help suppress combustion. Raman analysis confirmed an increased degree of graphitization in the residual carbon after UV irradiation polymerization grafting, indicating improved flame resistance. Overall, the synergy between char formation, silica-based insulation, and gas-phase flame retardancy enhanced the flame resistance of the modified PET fabric.

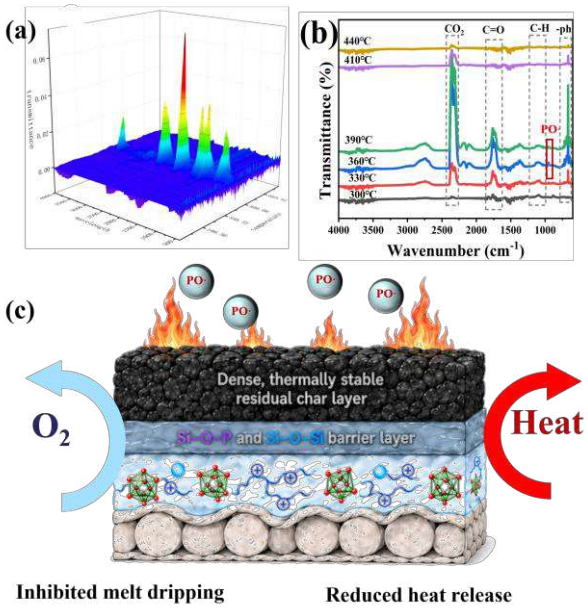


Fig. 9. TG-IR analysis during thermal decomposition: three-dimensional (3D) TG-IR spectra of (a) PET@PIL@SiO_2; (b) Two-dimensional (2D) correlation plots of mass change and infrared

absorption for PET@PIL/Nano SiO_2; (c) Schematic illustration of the condensed-phase flame-retardant mechanism.

4. Conclusions

In this work, PIL was used as the primary flame-retardant component, while inorganic Nano SiO_2 and organic POSS were introduced separately as synergistic silicon-containing FRs. Introducing PIL promoted catalytic carbonization of PET fabrics during combustion, reducing heat release and increasing char residue. At a PIL grafting ratio of 22.73 *wt*%, the PHRR of PET@PIL decreased by 25.54%, indicating the char-forming ability of the phosphorus-containing ionic liquid. However, the PET@PIL system still suffered from serious melt dripping during combustion, suggesting that PIL alone was insufficient to effectively suppress the melting behavior of PET fabrics. For the inorganic silicon-PIL system, Nano SiO_2 exhibited high thermal stability and nonflammability. During combustion, Nano SiO_2 mainly remained in the condensed phase and cooperated with the PIL-induced char layer to form a thermally stable Si-O-Si inorganic barrier. This barrier effectively inhibited heat transfer, oxygen diffusion, and the release of combustible volatiles, resulting in a significant reduction in heat release. In particular, PET@(PIL/Nano SiO_2(25%)) showed a reduction of 38.7% and 12.7% in PHRR and THR, respectively and no melt droplets were generated, compared with pristine PET. These results demonstrate that inorganic Nano SiO_2 has clear advantages in enhancing condensed-phase barrier protection, improving char stability, and suppressing heat release. Nevertheless, because Nano SiO_2 was mainly incorporated through physical blending, its interfacial compatibility with the organic PIL coating was still limited.

In contrast, organic POSS showed a different flame-retardant effect. Owing to its reactive organic groups, POSS could participate in free-radical polymerization and be covalently incorporated into the PIL molecular chain, forming an integrated phosphorus-silicon synergistic flame-retardant network. Although POSS was less effective than Nano SiO_2 in reducing heat release and smoke production due to its organic substituents and relatively lower inorganic silicon content, it exhibited a distinct advantage in improving coating stability and suppressing melt dripping. When the

IL/POSS feeding molar ratio was 1:0.75, PET@(PIL-*co*-PPOSS) achieved a UL-94 V-0 rating without melt dripping, and its LOI value increased to 23%.

Char morphology, Raman, and TG-IR analyses further confirmed the different roles of the two silicon-containing FRs. Nano SiO_2 mainly functioned as an inorganic condensed-phase barrier, contributing to heat insulation and char stabilization. POSS, however, contributed to the formation of a more integrated Si-O-P protective network due to its copolymerizable organic-inorganic hybrid structure. Meanwhile, PIL promoted dehydration, crosslinking, and carbonization in the condensed phase, while phosphorus-containing active fragments and nonflammable gases such as NH_3, N_2, and H_2O contributed to gas-phase flame inhibition.

Overall, silica-containing FR could be efficiently combined with IL to get enhanced fire resistance and anti-dripping behavior for PET fabrics. Nano SiO_2 was more effective in suppressing heat release and reinforcing condensed-phase barrier protection, while POSS was more beneficial for constructing an integrated phosphorus–silicon flame-retardant network, improving coating stability, anti-dripping behavior, and vertical burning performance.

Acknowledgements

This work was supported by the Beijing Natural Science Foundation (Grant No. 2242033), the Beijing Municipal Education Commission Outstanding Young Talent Program (Grant No. BPHR202203064), the Beijing Association for Science and Technology Youth Talent Support Program (Grant No. BYESS2023034), the Beijing Scholar Program (Project No. RCQJ20303) and General Projects of Graduate Education Quality Improvement (Project No. NHFZ20250420).

References

[1] Basak S, Waghmare A, Gupta D, et al. Effect of sodium ligno-sulphonate on flammability of PET woven fabric[J]. Journal of Industrial Textiles, 2023, 53: 15280837221150203.

[2] Üreyen M E, Kaynak E. Effect of Zinc Borate on Flammability of PET Woven Fabrics[J]. Advances in Polymer Technology, 2019, 2019(1): 7150736.

[3] Wang H, Sun L, Wang S, et al. A novel flame-retardant system toward polyester fabrics: flame retardant, anti-dripping and smoke suppression[J]. Journal of Polymer Research, 2022, 29(5): 180.

[4] Gu W, Dong Z, Zhang A, et al. Functionalization of PET with carbon dots as copolymerizable flame retardants for the excellent smoke suppressants and mechanical

properties[J]. Polymer Degradation and Stability, 2022, 195: 109766.
[5] Yi F, Zhu C J, Chen L, et al. High-performance flame-retardant PET copolyesters enabled by hydrogen-bonding and phosphorus-nitrogen synergism[J]. Polymer Degradation and Stability, 2025, 240: 111451.
[6] Bai Z, Wang Z, Wu D, et al. A thermostable phosphorus/nitrogen-based flame retardant with enhanced compatibility with PET[J]. Polymer Degradation and Stability, 2023, 218: 110581.
[7] Wang M, Yu B, Han J, et al. The influence of drawing pressure on the properties of PET/PA6 bicomponent spunbonded fibers[J]. Journal of Industrial Textiles, 2017, 46(5): 1281-1293.
[8] Tao Y, Liu C, Li P, et al. A flame-retardant PET fabric coating: Flammability, anti-dripping properties, and flame-retardant mechanism[J]. Progress in Organic Coatings, 2021, 150: 105971.
[9] Fang Y, Liu X, Tao X. Intumescent flame retardant and anti-dripping of PET fabrics through layer-by-layer assembly of chitosan and ammonium polyphosphate[J]. Progress in Organic Coatings, 2019, 134: 162-168.
[10] Pan Y, Liu L, Song L, et al. Durable flame retardant treatment of polyethylene terephthalate (PET) fabric with cross-linked layer-by-layer assembled coating[J]. Polymer Degradation and Stability, 2019, 165: 145-152.
[11] He Q, Wang J, Wang G, et al. Construction of a durable superhydrophobic flame-retardant coating on the PET fabrics[J]. Materials & Design, 2023, 233: 112258.
[12] Zhao W, Liu Y, Jiang L, et al. Preparation of flame retardant and anti-dripping PET fabric based on sodium copper chlorophyllin dyeing, UV grafting and phosphorylation[J]. Progress in Organic Coatings, 2024, 188: 108179.
[13] Ebdon J R, Price D, Hunt B J, et al. Flame retardance in some polystyrenes and poly(methyl methacrylate)s with covalently bound phosphorus-containing groups: initial screening experiments and some laser pyrolysis mechanistic studies[J]. Polymer Degradation and Stability, 2000, 69(3): 267-277.
[14] Jin J, Tang M, Zhang Z, et al. Synthesis of POSS-functionalized liquid crystalline block copolymers via RAFT polymerization for stabilizing blue phase helical soft superstructures[J]. Polymer Chemistry, 2018, 9(16): 2101-2108.
[15] Yang X, Liu X, Yang X, et al. A phosphorous/nitrogen-containing flame retardant with UV-curing for polyester/cotton fabrics[J]. Cellulose, 2022, 29(2): 1263-1281.
[16] Wang T, Li L, Cao Y, et al. Preparation and flame retardancy of castor oil based UV-cured flame retardant coating containing P/Si/S on wood surface[J]. Industrial Crops and Products, 2019, 130: 562-570.
[17] Hu Q, Wang W, Ma T, et al. Anti-UV and hydrophobic dual-functional coating fabrication for flame retardant polyester fabrics by surface-initiated PET RAFT technique[J]. European Polymer Journal, 2022, 173: 111275.
[18] Qi P, Wang W, Guo M, et al. Fabrication of P(DEMMP-*co*-VBImBF4) flame retardant and anti melt dripping nano coating onto polylactic acid fabrics via surface-initiated PET RAFT[J]. Polymer Degradation and Stability, 2026, 244: 111790.
[19] Li M, Sun A, Wang W, et al. A versatile ionic liquid functionalized macromolecular nano-coating via surface-initiated PET-RAFT: Imparting flame

retardancy, anti-dripping, and smoke suppression to polyester fabrics[J]. Colloids and Surfaces A: Physicochemical and Engineering Aspects, 2026, 737: 139665.
[20]Ren Y, Gu Y, Zeng Q, et al. UV-induced surface grafting polymerization for preparing phosphorus-containing flame retardant polyacrylonitrile fabric[J]. European Polymer Journal, 2017, 94: 1-10.
[21]Yu L, Zhang S, Liu W, et al. Improving the flame retardancy of PET fabric by photo-induced grafting[J]. Polymer Degradation and Stability, 2010, 95(9): 1934-1942.
[22]Özer M S, Gaan S. Recent developments in phosphorus based flame retardant coatings for textiles: Synthesis, applications and performance[J]. Progress in Organic Coatings, 2022, 171: 107027.
[23]Gu W, Wei L, Ma T, et al. Carbon Dots as smoke suppression agents for the reduction of CO release in combustion and improvement of UV resistance towards Phosphorus-containing polyester[J]. European Polymer Journal, 2022, 181: 111642.
[24]Ma T, Wang R, Wang W, et al. Studies on the thermal degradation mechanism of polyethylene terephthalate and its 2-carboxy ethyl (phenyl) phosphinic acid copolymers[J]. Polymer Degradation and Stability, 2022, 206: 110185.
[25]Jiang Q, Hu H, Sun J, et al. Intrinsically flame-retardant and biodegradable DDP-based adhesives for wet environments[J]. Chemical Engineering Journal, 2025, 515: 163938.
[26]Guo D ming, Jing X ke, Wu J ning, et al. Synthesis and characterization of a flame-retardant and anti-dripping copolyester[J]. Acta Polymerica Sinica, 2012, 012(9): 1042-1046.
[27]Sefa D C, Özmen F K, Üreyen M E, et al. Synthesis and Characterizations of DOPO Substituted Polyesters[J]. ChemistrySelect, 2025, 10(20): e01402.
[28]Özer M S, Wesemann M J, Gaan S. Flame retardant back-coated PET fabric with DOPO-based environmentally friendly formulations[J]. Progress in Organic Coatings, 2023, 175: 107363.
[29]Du J, Fan X, Xin F, et al. Novel coating flame retardant APP@UiO for preparation of flame retardant unsaturated polyester resin composites[J]. European Polymer Journal, 2024, 207: 112820.
[30]Chu F, Zhou X, Mu X, et al. An insight into pyrolysis and flame retardant mechanism of unsaturated polyester resin with different valance states of phosphorus structures[J]. Polymer Degradation and Stability, 2022, 202: 110026.
[31]Hamdani S, Longuet C, Perrin D, et al. Flame retardancy of silicone-based materials[J]. Polymer Degradation and Stability, 2009, 94(4): 465-495.
[32]Wang X, Zhang W, Qin Z, et al. Optically transparent and flame-retarded polycarbonate nanocomposite based on diphenylphosphine oxide-containing polyhedral oligomeric silsesquioxanes[J]. Composites Part A: Applied Science and Manufacturing, 2019, 117: 92-102.
[33]Nozari B, Montazer M, Mahmoudi Rad M. Stable ZnO/SiO_2 nano coating on polyester for anti-bacterial, self-cleaning and flame retardant applications[J]. Materials Chemistry and Physics, 2021, 267: 124674.
[34]Ye X, Zhang W, Yang R, et al. Facile synthesis of lithium containing polyhedral oligomeric phenyl silsesquioxane and its superior performance in transparency, smoke

suppression and flame retardancy of epoxy resin[J]. Composites Science and Technology, 2020, 189: 108004.
[35]Zhou Y, Hu Q, Wang W, et al. Controlled architecture of polyhedral oligomeric silsesquioxane-functionalized poly(glycidyl methacrylate)/polyester composites using surface-initiated ICAR ATRP Technique for High Flame Retardancy and Smoke Suppression[J]. Polymer Degradation and Stability, 2022, 199: 109914.
[36]Nagarajan S, Hwang S, Jaye C, et al. Investigation of electrode-electrolyte interfaces to enable non-flammable Li-ion batteries operating up to 125°C with liquid electrolyte[J]. Cell Reports Physical Science, 2025, 6(5): 102597.
[37]Wang Y, Xie T, Zhang J, et al. Green fabrication of an ionic liquid-activated lignocellulose flame-retardant composite[J]. Industrial Crops and Products, 2022, 178: 114602.
[38]Wang Y, Ren J, Ou M, et al. Flame-retardant and antibacterial properties of cotton fabrics treated by epichlorohydrin-modified aramid nanofibers, ionic liquid, and Cu ion[J]. Polymer Degradation and Stability, 2023, 212: 110347.
[39]Ou M, Lian R, Cui J, et al. Co-curing preparation of flame retardant and smoke-suppressive epoxy resin with a novel phosphorus-containing ionic liquid[J]. Chemosphere, 2023, 311: 137061.
[40]Chen Y, Wu W, Zhang M, et al. TGA-FTIR and char residue analysis: studying the synergistic flame retardancy mechanism of ionic liquid-modified graphene and hexaphenoxy cyclotriphosphazene[J]. Journal of Thermal Analysis and Calorimetry, 2022, 147(23): 13253-13259.
[41]Xie H, Basu S, DeMeter E C. Molecular Dynamics Simulations of Photo-Induced Free Radical Polymerization[J]. Journal of Chemical Information and Modeling, 2020, 60(12): 6314-6327.
[42]Holland B J, Hay J N. The thermal degradation of PET and analogous polyesters measured by thermal analysis–Fourier transform infrared spectroscopy[J]. Polymer, 2002, 43(6): 1835-1847.

Supplementary Files

This is a list of supplementary files associated with this preprint. Click to download.

- Supplementarymaterial.docx